Effects of annealing on the ferromagnetism and photoluminescence of Cu-doped ZnO nanowires



2010 J. Phys.: Condens. Matter 22 016002

(http://iopscience.iop.org/0953-8984/22/1/016002)

J. Phys.: Condens. Matter **22** (2010) 016002 (10pp) doi:10.1088/0953-8984/22/1/016002

# Effects of annealing on the ferromagnetism and photoluminescence of Cu-doped ZnO nanowires

**H J Xu[1], H C Zhu[1], X D Shan[1], Y X Liu[2], J Y Gao[1], X Z Zhang[1], J M Zhang[1], P W Wang[1], Y M Hou[1] and D P Yu[1]**

[1] State Key Laboratory for Mesoscopic Physics, Department of Physics, Peking University, Beijing 100871, People's Republic of China
[2] Key Laboratory for Magnetism and Magnetic Materials of the Ministry of Education, Lanzhou University, Lanzhou, Gansu 730000, People's Republic of China

E-mail: ymhou@pku.edu.cn and yudp@pku.edu.cn

Received 24 September 2009
Published 2 December 2009
Online at stacks.iop.org/JPhysCM/22/016002

**Abstract**
Room temperature ferromagnetic Cu-doped ZnO nanowires have been synthesized using the chemical vapor deposition method. By combining structural characterizations and comparative annealing experiments, it has been found that both extrinsic (CuO nanoparticles) and intrinsic ($Zn_{1-x}Cu_xO$ nanowires) sources are responsible for the observed ferromagnetic ordering of the as-grown samples. As regards the former, annealing in Zn vapor led to a dramatic decrease of the ferromagnetism. For the latter, a reversible switching of the ferromagnetism was observed with sequential annealings in Zn vapor and oxygen ambience respectively, which agreed well with previous reports for Cu-doped ZnO films. In addition, we have for the first time observed low temperature photoluminescence changed with magnetic properties upon annealing in different conditions, which revealed the crucial role played by interstitial zinc in directly mediating high $T_c$ ferromagnetism and indirectly modulating the Cu-related structured green emission via different charge transfer transitions.

(Some figures in this article are in colour only in the electronic version)

## 1. Introduction

Dilute magnetic semiconductors (DMSs) have attracted a great deal of attention in recent years, with the focus on manipulating both the charge and the spin of the electrons [1, 2]. Among these DMS materials, transition metal (TM)-doped ZnO is a particularly promising candidate for future spintronics application, since its Curie temperature ($T_c$) is predicted to be well above room temperature [3, 4]. Although room temperature ferromagnetism (RTFM) of TM-doped ZnO has been reported in a large number of studies [5–8], the origins of such RTFM remain controversial, both in theory and experiments.

In theory, there are two main explanations of the RTFM in DMSs, namely, the carrier-mediated mechanism [3, 9] and percolation of bound magnetic polarons (BMP) [10, 11]. A hole-mediated mechanism was firstly employed by Dietl *et al* [3] to predict high $T_c$ for p-type TM-doped wide bandgap DMSs, where a large density of mobile holes are required to induce the sufficient ferromagnetic exchange interaction among TM dopants. This was later partly verified by experimental observations of RTFM in TM-doped $TiO_2$ and ZnO [5, 12, 13]. However, n-type carriers and their relatively low concentration challenged such theory [12, 14, 15]. As a result, a spin-split impurity band theory derived from the BMP model was proposed by Coey *et al* [11], in which the shallow donors regulate the dopant magnetic moment alignment in n-type wide bandgap DMSs. In order to activate the RTFM, the donor electrons in the impurity band should delocalize onto TM dopants, remarkably increasing the donor–dopant coupling, i.e. the empty TM 3d states have to hybridize with the donor states at the Fermi level. In any case, the type, mobility and concentration of the carriers have a significant impact on the magnetic properties, which provide an opportunity to manipulate the ferromagnetism of DMSs. On the other hand, annealing under appropriate conditions can modulate the

 

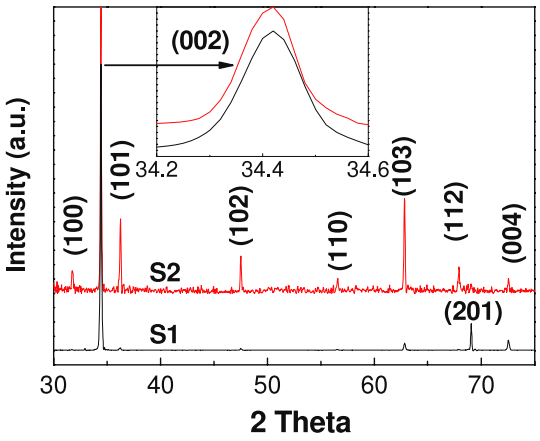


**Figure 1.** XRD patterns of as-grown undoped ZnO NWs (sample S1) and Cu-doped ZnO NWs (sample S2). The inset shows their magnified (002) peaks.

intrinsic point defects of the TM-doped DMSs and influence the properties of the carriers to regulate the magnetism, as has been reported widely [16–18]. In addition, for Cu-doped ZnO [19–21], its saturation magnetic moment ($M_s$) would increase significantly upon annealing in Zn vapor and decrease considerably upon annealing in oxygen ambience.

In experiments, the most critical issue is whether the RTFM originates from an intrinsic or extrinsic source such as a secondary magnetic phase or clusters [22–24]. At room temperature, copper and its oxides are generally considered to be nonmagnetic [25, 26], and Cu-doped ZnO possesses a ferromagnetic ground state suggested by several first-principles calculations [27, 28]. Many studies of Cu-doped ZnO have been undertaken recently and RTFM was observed [29, 30]. Avoiding the 'pollution' of a ferromagnetic secondary phase, RTFM was attributed to the intrinsic properties. However, some reports [31, 32] demonstrated that a nanophase of CuO may also generate RTFM, although bulky CuO is nonmagnetic. As a result, the exact origin of the ferromagnetism in Cu-doped ZnO is currently a controversial issue and needs profound investigations [33].

Until now, most of the experiments have concentrated on films. As a basic building block in nanotechnology, NWs should be paid more attention because their dimensionality and size may significantly modulate their properties, making them distinct from their bulk partner [34]. Besides, TM-doped ZnO NWs, being single crystalline, single domain, and single phase, serve as an excellent model system for investigating structures and their correlation with properties in order to elucidate the origin of RTFM [35]. Here, we report the effects of annealing on the magnetic properties of Cu-doped ZnO NWs prepared by the CVD method. The as-grown samples exhibited robust RTFM. For the reasons mentioned above, we believe annealing offers a simple but feasible technique for testing whether the ferromagnetism is an intrinsic property of the DMS in the absence of some special equipment, such as magnetic circular dichroism (MCD). After systematic comparative annealing experiments, we assigned the large proportion of the FM to the nanoparticles (NPs) of CuO (diameters ∼5 nm) on the surface of Cu-doped ZnO NWs. Such NPs could not be detected by means of x-ray diffraction (XRD), but can be observed directly in high resolution transmission electron microscopy (HRTEM) and this was confirmed by x-ray photoelectron spectroscopy (XPS), whereas small parts of the FM, which can be reversibly changed by consecutive annealings in Zn vapor and oxygen ambience, were ascribed to the intrinsic ferromagnetic $Zn_{1-x}Cu_xO$ nanowires ($x \sim 1\%$). A low temperature (10 K) photoluminescence (PL) technique was employed to study the intrinsic point defects and electronic structure of the system. More importantly, we found direct evidence of interstitial zinc ($Zn_i$) in regulating both the ferromagnetism and the well-known Cu-related structured green emission (SGE) in Cu-doped ZnO. A self-consistent explanation was eventually given for these reversible effects of annealing on the PL and FM of Cu-doped ZnO NWs under the framework of spin-split impurity band theory.

## 2. Experiments

The precursor substances for Cu-doped ZnO NWs are a mixture of zinc powders (purity ∼99.999%) and copper NPs (diameter: 100–200 nm). Due to the size effect [36], the copper NPs can vaporize at relatively low temperature, 600–700 °C, in spite of the fact that the melting point of bulk copper is higher than 1000 °C. These Cu particles are synthesized by adding appropriate amounts of Zn powders into the $CuCl_2$ solution via the following chemical reaction: $Zn + Cu^{2+} \rightarrow Zn^{2+} + Cu$. After the reaction, washing these materials with deionized water several times, and vaporizing the residual water at low temperature and low pressure, we finally obtained the expected NPs composed of copper, zinc and their oxides without any other pollution, examined using XPS. For the undoped ZnO NWs, only zinc powders were used.

Both the undoped and Cu-doped ZnO NWs were synthesized in a typical horizontal furnace as described in previous work by our lab [37]. Zn powders and Cu nanopowders with a weight ratio of 5:1 (∼0.5 g in all) were ground together and pushed into the furnace after it had reached the desired temperature, 650 °C, and Ar (99.999%, 100 sccm) was introduced; we then evacuated the furnace to the ultimate pressure (∼Pa), and 5 min later added $O_2$ (99.999%, 0.5 sccm). The reaction lasted for 20 min. After cooling down, a gray or brown deposition layer was found over those Si(100) substrates.

In the Zn vapor annealing experiments, the samples were carefully half-wrapped with high purity Zn foil (99.99%), and then laid on the Zn powders (∼1 g) inside a quartz cuvette. We kept the temperature of the furnace at 420 °C for 5 h and protected it in Ar ambience with a pressure a little higher than atmospheric. For the annealings in oxygen ambience, we exposed samples to oxygen ambience and kept the temperature at 600 °C for 1 h under pressure higher than that outside.

SEM (Quanta 200FEG), XRD (Rigaku Dmax/2000) and TEM (Tecnai F30) techniques were employed to study the morphology and crystal structure of the as-grown sample. The XPS (AXIS-Ultra instrument, from Kratos Analytical,

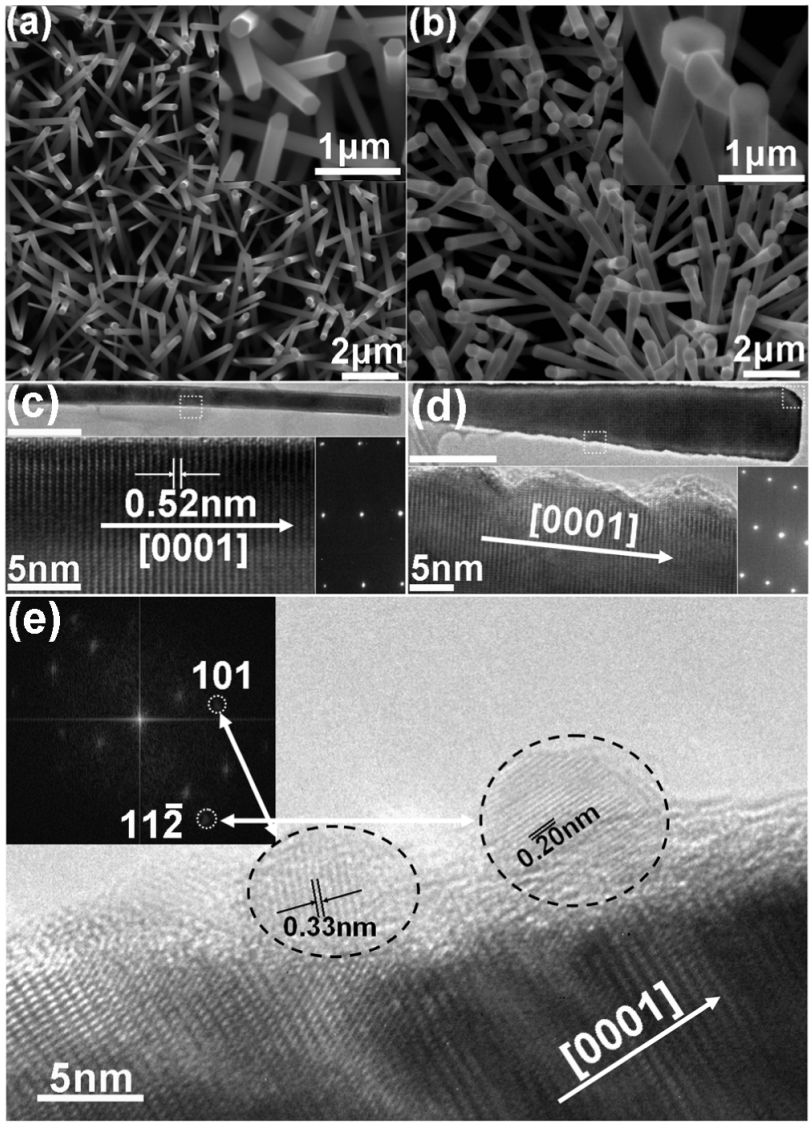


**Figure 2.** ((a), (b)) SEM images of as-grown samples S1 and S2, respectively. The insets show magnified images of their local morphologies. ((c), (d)) TEM images (upper parts) of individual undoped ZnO and Cu-doped ZnO nanowires, respectively, with HRTEM images (lower parts) of their boundary parts. The images lower right show their SAED patterns without a secondary phase being detected. (e) HRTEM image at the tip of Cu-doped ZnO NW shown in figure 1(d), including two CuO NPs. The inset displays the corresponding FFT image, in which two extra spots can be identified as {101} and {11$\bar{2}$} planes of monoclinic CuO.

using monochromatic Al K$\alpha$ radiation) spectrum was utilized to further explore the detailed constitution of the sample. Room temperature magnetic properties are investigated using an alternating gradient magnetometer (AGM, Model 2900, Princeton Measurement Corporation) which has nearly the same precision ($\sim 10^{-8}$ emu) as a superconducting quantum interference device magnetometer. From the PL analysis, excited by a 325 nm wavelength He–Cd laser, we got information about these intrinsic point defects and the state of the Cu atoms in the ZnO lattice.

## 3. Results and discussion

### *3.1. Structure characterization*

XRD studies were conducted to investigate the integral structures of as-grown samples. Undoped (S1) and Cu-doped (S2) ZnO NWs were synthesized in the same conditions (figure 1). All the peaks correspond to the wurtzite structure of ZnO (SG $P63mc$, $a = 0.325$ nm, $c = 0.521$ nm). Within the detection limit of the XRD technique, there are no detectable peak shifts between S1 and S2. However, these two samples show different morphologies. NWs in S1 (figure 2(a)) are denser but thinner than NWs in S2 (figure 2(b)). The diameters and lengths of undoped ZnO NWs are in the ranges of 100–300 nm and 5–10 $\mu$m respectively, with uniform hexagonal cross-section and smooth surfaces, while the diameters of Cu-doped ZnO NWs ($\sim$10 $\mu$m in length) gradually become larger from $\sim$200 nm at the bottom to $\sim$400 nm at the top. Some Cu-doped ZnO NWs show deformed hexagon sections, and in particular hole-like defects at the tips, which may be induced by doping. According to HRTEM analysis, these NWs, no matter whether the sample was undoped or

doped, all grew along the [0001] direction. The undoped ZnO NW (figure 2(c)) exhibits homogeneous and defect free crystalline structures with a clear surface, whereas the doped ZnO NW (figure 2(d)) has poorer crystallinity with a rough surface. More importantly, some CuO NPs (diameter ∼5 nm) were found by carefully examining the tip of the NW (see figures 2(d) and (e)), although no trace of a secondary phase was observed in the selected area electron diffraction (SAED) pattern. We recognized these NPs as CuO for the following two reasons. First, more Cu content was detected in this area around these particles by employing an energy dispersive x-ray (EDX) element analysis. Second, these interplanar spacings of 0.33 nm and 0.20 nm can be indexed to {101} and {11$\bar{2}$} planes of monoclinic CuO respectively, by utilizing the fast Fourier transform (FFT) of the corresponding HRTEM image shown in figure 2(e).

XPS analysis was carried out to determine the doping concentration and the valence state of Cu in the ZnO matrix (S2). The survey scan (figure 3(a)) shows only three elements: oxygen, zinc and copper (carbon comes from the inevitable pollution). After quantitative analysis, we found that their atomic composition percentages are 59.6, 34.6, and 5.8 at.% respectively, with the percentage of Cu atoms in all cations surprisingly up to 14.36 at%. Actually, XPS measurement only gives composition information for the surface (depth of several nanometers). In order to further explore the composition of the internal lattices, Ar ions were employed to etch the sample to a depth of ∼50 nm from the surface. We found that the content of doped Cu was only 1.37 at%, as shown in the inset of figure 3(a). Since this concentration is more reasonable, it was used to calculate the average magnetic moment per Cu atom for the doped ZnO. This result reveals that Cu atoms have a tendency to aggregate at the surface of ZnO NWs as reported previously [38], which may result from the very low solid solubility of Cu in ZnO. For the surface, it is shown that the Cu $2p_{3/2}$ and Cu $2p_{1/2}$ peaks locate at 933.32 and 953.15 eV respectively, which corresponds to a mixed oxidation state of +1 and +2 for Cu. The Gaussian fitted curve (figure 3(b)) gives a major $Cu^{2+}$ component (∼71 at.%, from fixing the $2p_{3/2}$ peak at 933.6 and the $2p_{1/2}$ peak at 953.5) and a minor $Cu^{1+}$ component (∼29 at.%, from fixing the $2p_{3/2}$ peak at 932.6 and the $2p_{1/2}$ peak at 952.5) [39]. Furthermore, the appearance of a peak about 10 eV above the main $2p_{3/2}$ peak, known as a shake-up satellite [40], reveals the existence of the CuO phase on the surface of Cu-doped ZnO NWs. The size of typical CuO NPs deduced from HRTEM is rather small, which results in an amazing effect in magnetism as will be shown in a later section.

Aiming to explore the local structure of the Cu atoms, their charge state in the ZnO lattice and the intrinsic point defects of the host, PL experiments were carried out (figure 4). The inset of figure 4(a) shows the room temperature PL spectra of the as-grown samples. S1 possesses a strong near band edge UV emission together with negligible visible emission, which means that these undoped NWs have a fairly good crystallinity. In contrast, S2 has a high intensity of green emission which was possibly due to intrinsic defects (such as $V_O$ [41]) or extrinsic defects ($Cu_{Zn}$). Its near band edge

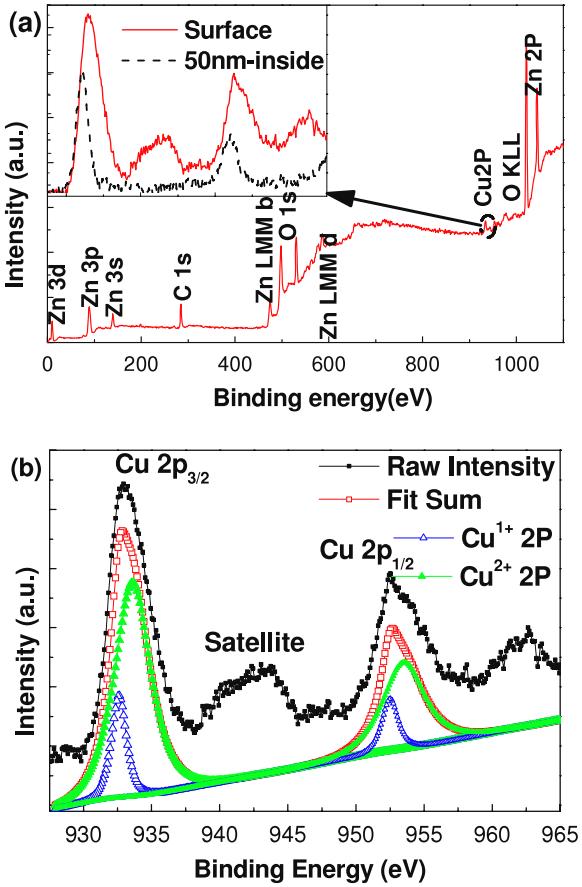


**Figure 3.** XPS spectrum of Cu-doped ZnO (S2) NWs. (a) Survey scan of the sample; the inset shows the high resolution scan of the copper 2p peaks before and after Ar ion etching. (b) Gaussian fitting of the copper 2P peaks (before etching) with $Cu^{2+}$ and $Cu^{1+}$ components.

emission is depressed severely because of Cu doping, as in earlier reports on TM doping [42]. Besides, for S2 its PL intensity was magnified to 15 times, which means that the PL was afflicted with doping because of the poorer crystallinity and greater level of structural defects. The exciton emissions (figure 4(a), 10 K) of S1 and S2 show that each of them displays a prominent peak in the range of 3.35–3.37 eV which is assigned to the neutral donor bound excitons ($D^0X$) [43] caused by certain shallow donors, such as $H_i$, $Zn_i$ and $Ga_{Zn}$. The most intensive $D^0X$ of S1 locates at 3.362 eV with a dominant intensity, while S2 displays a much weaker $D^0X$ at around 3.358 eV (about one thousandth of that for S1 in intensity). This striking difference can be understood by comparison with the different transport properties of undoped ZnO and Cu-doped ZnO. According to [29], after Cu was doped into n-type ZnO, the carrier density would be diminished by several orders of magnitude. Assuming that the $D^0X$ intensity is proportional to the concentration of shallow donors at low temperature and all the shallow donors can ionize at room temperature will yield the same result as these transport experiments. In addition, the Cu-doped ZnO NWs display the well-known SGE [44], yet the undoped ZnO NWs exhibit a weaker structureless green emission [45, 46]. For the SGE,

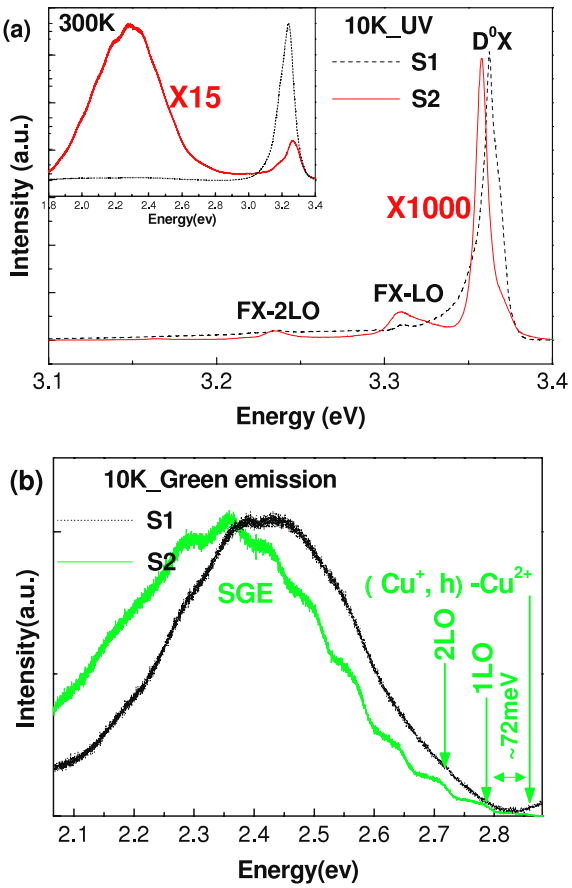


**Figure 4.** Photoluminescence (PL) spectra of as-grown samples S1 and S2, respectively. (a) Low temperature (10 K) exciton emissions. The inset shows their room temperature PL spectra. (b) Green emission (10 K). CTT emission $(Cu^{+}, h) \rightarrow Cu^{2+}$ and its phonon replicas bring about the structured green emission (SGE), denoted by the green arrowhead.

it was first suggested by Dingle [44] that the charge transfer transition (CTT) from ($Cu^{+}$, h), a complex made up of $Cu^{+}$ and a loosely bound hole, to the $3d^9$ ground state $Cu^{2+}$ gives rise to the no-phonon line at ∼434 nm (2.859 eV). This no-phonon line together with its longitudinal optical (LO) phonon replicas (∼72 meV interval) leads to the SGE band illustrated in figure 4(b). Dingle claimed that the association of the SGE with a divalent copper ion on a zinc lattice site must be established. Further experiments and theoretical models confirmed his suggestion [47, 48]. Therefore, the clear SGE band in our samples validates that Cu atoms substitute for the Zn atoms with a state of $Cu_{Zn}$, which is the precondition for the generation of intrinsic RTFM in Cu-doped ZnO systems.

### *3.2. Magnetic and optical properties*

From magnetic measurements on samples S1 and S2 at room temperature, a clear hysteresis loop was found only for S2. The as-grown Cu-doped ZnO NWs exhibited an $M_s$ of ∼0.2 $\mu_B$/Cu and coercivity ($H_c$) of about 50 Oe, which is within the range of experimental results reported for Cu-doped ZnO films [49, 50]. Because undoped ZnO samples grown in the same conditions did not display any RTFM, it was concluded that the RTFM in S2 was Cu related. However, the question arises of whether this ferromagnetism originates from an intrinsic or an extrinsic source.

As an intrinsic property, the ferromagnetism of Cu-doped ZnO should be evaluated by means of annealing in Zn vapor or oxygen ambience [19–21]. S2 was first annealed in Zn vapor at 420 °C for 5 h. Unexpectedly, the net magnetic moment of the annealed sample dramatically decreased to about 10% of that of the as-grown sample, as figure 5(a) shows. After that, we put the Zn vapor annealed sample into oxygen ambience at 600 °C for 1 h, and found that the FM almost disappeared. A favorable turning point occurred when we exposed the sample to Zn vapor again, as displayed in figure 5(b). The sample returned to showing FM with a much weaker magnetic moment (∼0.011 $\mu_B$/Cu) as compared with the as-grown sample. This value is relatively low but comparable with the result of Wang *et al* [38]. More interestingly, when the specimen was annealed in oxygen ambience again, and then Zn vapor, the FM can be switched OFF and ON, which has been commonly found in many Cu-doped ZnO samples. Therefore these results definitely show that the specimen exhibited two different behaviors responding to annealings in Zn vapor, which may reveal the different origins.

For the large decrease in $M_s$ after the first Zn vapor annealing, considering the structure analysis, we tentatively ascribed the large $M_s$ of the as-grown sample to the CuO NPs and the decrease in $M_s$ as due to the change of CuO NPs. Although bulk CuO is nonmagnetic, the nanosize CuO (diameter ⩽10 nm) is likely to generate RTFM owing to the uncompensated spins of the surface metal ions [31, 51]. When annealed in Zn vapor, CuO NPs will be deoxidized by Zn atoms, and form supersmall Cu particles. Then these Cu particles evaporate easily and cause a significant decrease in $M_s$. In order to verify this proposal, we dispersed some high purity (99.9%) CuO NPs (diameter ∼50 nm) in ethanol by an ultrasonic process, and then dropped them onto the Si substrate. As expected, we got a strong FM in the as-prepared sample but a much weaker FM after Zn vapor annealing (the inset of figure 5(a)), which confirms our suggestion.

For the reversible magnetic behavior after annealing in Zn vapor for the second time, comparative experiments indicated that the changeable magnetic property in S2 was Cu related. As shown in figure 5(a), S1 was annealed in identical conditions with its nominal $M_s$ changed in an irregular way. Furthermore, we hold that it is connected with those Cu atoms doped into ZnO lattices. Because Cu has a low thermal equilibrium solid solubility in ZnO lattices, especially when the temperature is higher than 700 °C, doped Cu atoms will diffuse outwards from the ZnO lattices [23, 52]. After S2 was annealed in oxygen ambience at elevated temperature (900 °C) for 1 h, the FM undoubtedly disappeared. Nevertheless, after the following annealing in Zn vapor, the $M_s$ could not return to the previous value. Even if we extended the annealing time from 5 to 10 h, $M_s$ was just about half of the previous value. Due to the out-diffusion of Cu atoms, only part of them remained upon substitution of Zn atoms, bringing about much weaker ferromagnetism after successive annealings in 900 °$CO_2$ and Zn vapor. Up to here, we can attribute the reversible tuning

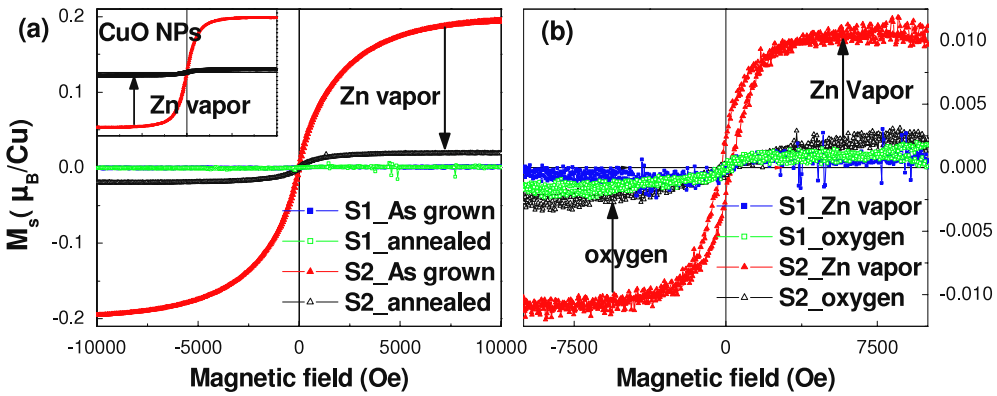


**Figure 5.** (a) Comparison of $M$–$H$ curves measured for the as-grown, Zn vapor annealed (for the first time) samples and CuO NPs (inset). Compared with that of S2, the magnetic moment of S1 is so small as to be negligible. (b) $M$–$H$ curves of S1 and S2 successively annealed in Zn vapor and oxygen ambience for the second time.

of ferromagnetism to an intrinsic property of Cu-doped ZnO safely. For one thing, to our knowledge, there have been few experiments [16, 53] that realized manipulating the FM in a reversible manner by consecutive annealings, and all of them had excluded the possibility of an extrinsic ferromagnetic source unambiguously. Likewise, we have previously proved that CuO cannot be responsible for such reversibly changeable behavior. For another, in our case this phenomenon should relate to $Zn_{1-x}Cu_xO$, whose existence was confirmed by the SGE. Suppose that it was caused by secondary phase segregation; Cu or Cu oxides should precipitate in the lattice of ZnO NWs. However, the single crystallinity of these individual NWs confirmed by SAED and HRTEM analysis rules out this possibility.

As annealing can change the intrinsic point defects of the host, low temperature PL measurements were performed on our doped samples to explore the role played by these point defects in tuning the magnetic properties. As illustrated in figure 6(a), all the PL spectra have a dominant peak $D^0X$, which suggests that the n-type property of the ZnO host did not change with annealing, while the position and intensity of $D^0X$ varied a lot with annealing. For the as-grown sample, the main $D^0X$ peak was positioned at 3.3577 eV with a medium intensity. We could not find the free exciton (FX) clearly, although its phonons were clearly observed (FX LO: ∼3.3091 eV, FX 2LO: ∼3.2353 eV). After S2 was annealed in Zn vapor, the $D^0X$ increased distinctly with a blue shift (3.3615 eV), and its two-electron satellite line (TES, 3.3336 eV) emerged. Using this formula [54], $E_D = (E_{D^0X} - E_{TES}) \times 4/3$, we can estimate the donor binding energy (∼37 meV). It was almost equal to the binding energy of $Zn_i$ reported by [55]. Besides this, it is worth noticing that the energy gap ($E_g$) had a blue shift deduced from the shift of the FX LO phonon (∼9 meV) of the Zn vapor annealed sample (∼3.3180 eV) compared with the as-grown sample (∼3.3091 eV). This result might originate from an increase of the shallow donor concentration and hence the increase of the $D^0X$ intensity according to the so-called Moss–Burstein shift theory [56]. After the following 600 °$CO_2$ annealing, an opposite change happened. $D^0X$ was suppressed obviously and red-shifted to 3.3599 eV with its weak TES

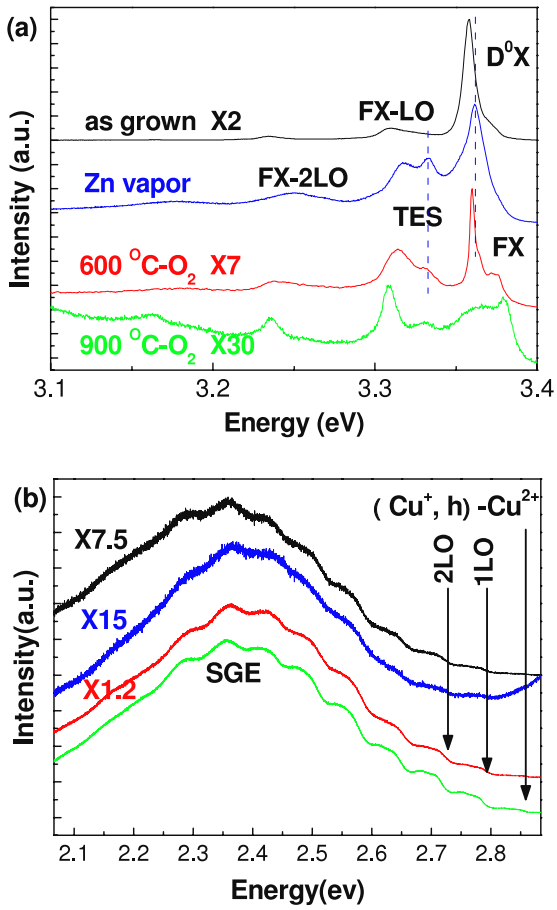


**Figure 6.** Comparison of 10 K PL spectra of S2 after annealings in different conditions. The curves correspond to the as-grown, Zn vapor annealed, 600 °$CO_2$ annealed and 900 °$CO_2$ annealed S2 respectively, from top to bottom. (a) Shows that $D^0X$ tends to increase upon annealing in Zn vapor but decrease upon annealing in $O_2$, whereas (b) reveals the opposite behaviors of SGE responding to the annealings.

peak located at 3.3319 eV. Once again, we got the same donor binding energy (∼37 meV). As a result, the shallow donor concentration is decreased upon annealing in oxygen ambience. This is merely a general property of ZnO annealed

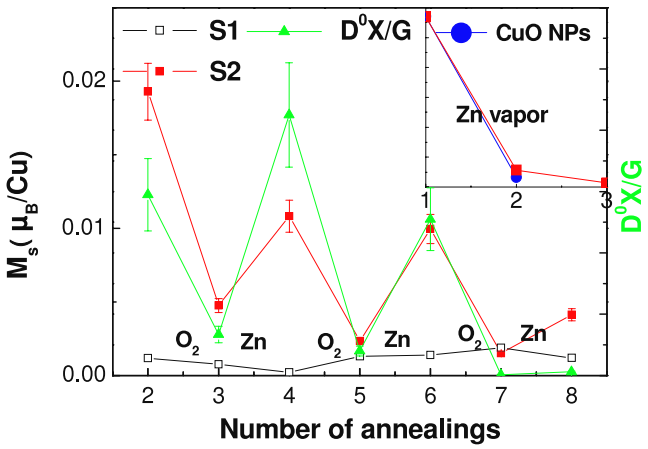


**Figure 7.** Variations of $M_s$ with the successive Zn–$O_2$ annealings for samples S1, S2 and CuO NPs; the last $O_2$ annealing was conducted at 900 °C. As a comparison, the ratio of $D^0X$ to G (green emission centered at 525 nm) is also displayed, which shows the same tendency as $M_s$ responding to annealings.

in oxygen ambience [20, 45, 57], and we confirmed it by low temperature PL analysis. Because of the identical donor binding energies, we identified these $D^0X$ as related to the same donor. $Zn_i$ is the most likely candidate. First, its donor binding energy is $\sim 30 \pm 5$ meV according to previous research [58], in good agreement with our result. Second, $Zn_i$ has a much lower diffusion obstacle, which makes it easy to produce and destroy at relatively low temperature [59]. To summarize, we assert that the controllable changes of $D^0X$ in the Zn–$O_2$ annealing experiments were caused by the introduction and removal of $Zn_i$. This conclusion is in accordance with existing reports [16, 60], and importantly, we found direct evidence for it from low temperature exciton emissions.

For the visible emission, a similar phenomenon was found (see figure 6(b)). The as-grown sample showed a clear SGE emitted by the CTT between $(Cu^+, h)$ and $Cu^{2+}$. After the sample was exposed to Zn vapor, the SGE tend to be smoothed, and this was accompanied with reduced intensity. Then returning the sample to 600 °$CO_2$ annealing, SGE recurred with significant intensity enhancement.

As stated above, the magnetic moment of S2 changed in the same manner as the intensity of the $Zn_i$-related $D^0X$ but in contrast to that of SGE responding to the successive Zn–$O_2$ annealings (see figure 7, where we display the ratio of $D^0X$ to G in order to lessen the system error). Therefore, the next question is how this relationship between the reversible ferromagnetic switching and the corresponding changes of LT PL spectra works. The intrinsic mechanism will be elucidated in the following section.

## 4. Discussion

In this work, the Cu-doped ZnO NWs are n-type on account of the prominent $D^0X$, without any acceptor-related peaks in the exciton emission spectra (10 K). Therefore, the spin-split impurity band theory should provide a rational explanation of our experiments; this calls for hybridization between empty TM 3d states and donor states at the Fermi level. On the basis of such theory, Kittilstved *et al* developed a criterion for evaluating high $T_C$ ferromagnetism by analyzing CTTs and extended this method to both n-type and p-type DMSs [61]—that is, the emergence of dopant-derived donor- or acceptor-type ionization states in close proximity to the band edge of n-type or p-type DMSs, respectively. In this section, we will analyze our results following their method.

As shown above, the presence of SGE means the occurrence of such CTTs:

$$Cu^{2+} + h\nu \leftrightarrow (Cu^+, h^+_{VB}), \tag{1}$$

where $h\nu \geqslant 2.859$ eV, and the hole, $h^+_{VB}$, is loosely bound to $Cu^+$ with binding energy $\varepsilon_1 \sim 0.390$ eV [47]. Thus, we get

$$(Cu^+, h^+_{VB}) + \varepsilon_1 \rightarrow Cu^+ + h^+_{VB} \tag{2}$$

$$Cu^{2+} + \varepsilon_2 \rightarrow Cu^+ + h^+_{VB}, \tag{3}$$

where $\varepsilon_2$ is $\sim$3.249 eV ($\varepsilon_2 = h\nu + \varepsilon_1$) and the reaction (3) is exactly the ligand valence band-to-metal charge transfer ($L_{VB}M^{2+}CT$) described in [61]. Hence, the following reaction ($M^+L_{CB}CT$) is deduced:

$$Cu^+ + \varepsilon_3 \rightarrow Cu^{2+} + e^-_{CB}. \tag{4}$$

We have $\varepsilon_3 \sim 0.186$ eV ($\varepsilon_3 = E_g - \varepsilon_2$), as $h^+_{VB} + e^-_{CB} = E_g \sim 3.435$ eV. This means that a shallow donor-type ionization state, $Cu^+$, exists in the Cu-doped ZnO system, whose donor binding energy is $\sim$0.186 eV (see figure 8) [62]. In the presence of other shallow donors, it is the key prerequisite for dopant–defect hybridization at the Fermi level and hence high $T_C$ FM [11]. Quantitatively, from perturbation theory the dopant–defect hybridization is inversely proportional to the energy difference between the dopant ($Cu^+$) and defect levels ($Zn_i$), $E_{DD}$. Noticing that the binding energy of the main donor ($Zn_i$) is about 0.037 eV for our sample, we get $E_{DD} \sim 0.149$ eV. This is really small compared with the value for Co-doped ZnO, $\sim$0.27 eV [61], which was small enough to generate the RTFM ($\sim$0.046 $\mu_B$/Co). According to the above criterion, because a donor-type ionization state ($Cu^+$) exists in close proximity to the band edge of the Cu-doped ZnO, the RTFM ($\sim$0.011 $\mu_B$/Cu) in our n-type Cu-doped ZnO NWs can be authenticated and is even likely to regulate the FM. However, for the comparatively weak ferromagnetism, it is possibly due to the low Cu concentration ($\sim$1%) and the existence of monovalent Cu atoms, which make no contribution to the magnetic moment.

According to spin-split impurity band theory, the shallow donor concentration must be large enough to trigger the paramagnetism–ferromagnetism (PM–FM) transition. On the other hand, as we have seen, the concentration of $Zn_i$ donors can be regulated by sequential Zn–$O_2$ annealings. Accordingly, the Cu-doped ZnO system became ferromagnetic when annealed in Zn vapor but paramagnetic in oxygen ambience. That is why $Zn_i$-related $D^0X$ and $M_s$ changed in the same manner.

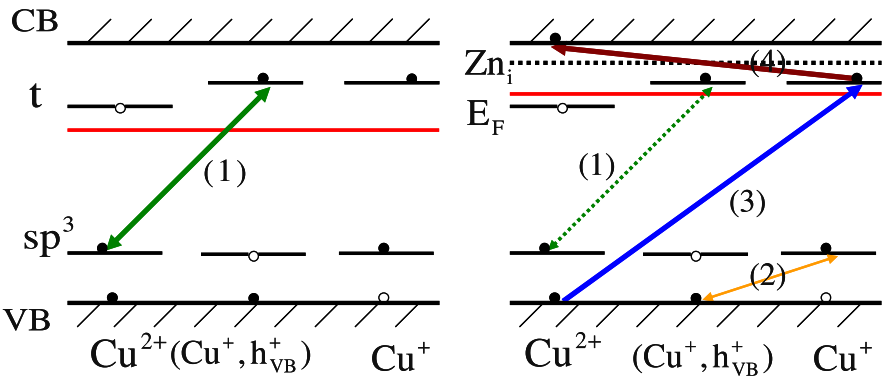


**Figure 8.** Energy levels of Cu ions in various charge states and the charge transfer transitions (CTTs) between them in Cu-doped ZnO after annealings in $O_2$ (left) and Zn vapor (right), respectively. For the former, because its low electron concentration Fermi energy ($E_F$) must lie below the t energy level of $Cu^{2+}$, (1), $Cu^{2+} + h\nu \leftrightarrow (Cu^+, h^+_{VB})$, is the main CTT process. For the latter, with the introduction of shallow donors $Zn_i$, $E_F$ should lie between the t energy levels of $Cu^{2+}$ and $Cu^+$ and hence the hybridization between $Cu^+$ and $Zn_i$ occurs with (3) $L_{VB}M^{2+}$ CT and (4) $M^+L_{CB}$ CT taking place. CB denotes conduction bands, VB, valence bands, t, the highest energy level of Cu 3d bands in the ZnO lattice, $sp^3$, hybrid states of Cu 4s with O 2p orbitals, and (2), the capture and release of $h^+_{VB}$ by $Cu^+$.

Actually, we can find more details about the process by analyzing the CTTs. It is noticed that in Dingle's model, isolated $Cu^{2+}$ is the ground state of the dopant ($Cu_{Zn}$) in the ZnO lattice [46]. This implies all the Cu atoms have no coupling with each other, i.e. they are paramagnetic. When excited by a photon ($E \geqslant 2.859$ eV), the hole in the 3d orbital of $Cu^{2+}(3d^9)$ transfers to the four oxygen atoms encompassed, and hence the complex ($Cu^+$, $h^+_{VB}$) forms. Because $Cu^{2+}$ (PM) is the thermodynamic equilibrium charge state for $Cu_{Zn}$, soon ($Cu^+$, $h^+_{VB}$) returns to the $Cu^{2+}$ state via a radiant recombination and gives out the SGE. That is exactly what happens in the Cu-doped ZnO system when it is in paramagnetic state after annealing in oxygen ambience. As a result, the intensity of SGE has a direct relationship with the number of isolated $Cu^{2+}$ occupied, i.e. paramagnetic $Cu^{2+}$. This conclusion is in accord with [63], in which the presence of SGE was attended by an electron paramagnetic resonance signal of $Cu^{2+}$. However, when enough shallow donors ($Zn_i$) were introduced by annealing in Zn vapor, such ionization will happen:

$$Zn_i + \varepsilon_b \rightarrow Zn_i^+ + e^-_{CB}, \tag{5}$$

where $\varepsilon_b$ is ~0.037 eV. Because of the relatively small $E_{DD}$, the reaction inverse to (4) takes place resonantly [61], which means that the shallow donor electrons delocalize onto $Cu^{2+}$. Then the $Zn_i$–$Cu^{2+}$ resonance will become approximately thermoneutral:

$$Zn_i{:}Cu^{2+}{:}ZnO \leftrightarrow Zn_i^+{:}Cu^+{:}ZnO. \tag{6}$$

Consequently, hybridization between $Cu^{2+}$ and the shallow donor impurity band occurs, leading to ferromagnetic coupling among those $Cu_{Zn}$ atoms as long as they are within the effective Bohr radius of the same donor (figure 9) according to the spin-split impurity band theory. That is to say, when the system is in the FM state, not isolated $Cu^{2+}$ but ferromagnetically coupled $Cu^{2+}$ together with $Cu^+$ becomes the thermodynamic equilibrium charge state for $Cu_{Zn}$. Thus, it is CTTs (3) and (4) not CTT (1) that are dominant; hence the SGE diminishes greatly. All these processes, including the magnetic and optical changes, are described in the schematic illustration shown in figures 8 and 9. It is worth mentioning that a similar phenomenon was reported in [7] and [16]. The strongest FM went with the strongest shallow donor IR absorption and the weakest ligand field absorption, which meant the largest concentration of shallow donors and the weakest PM respectively and vice versa.

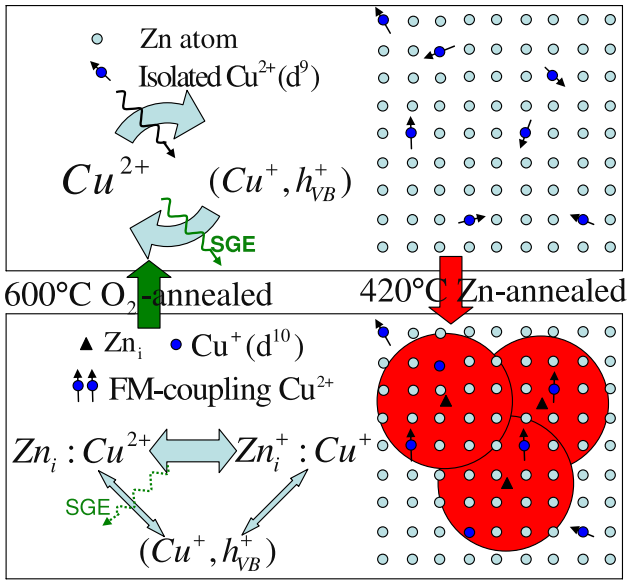


**Figure 9.** Schematic illustration of the annealing effects on optical and magnetic properties of Cu-doped ZnO NWs. After annealing in $O_2$ (600 °C), Cu atoms are isolated (paramagnetic state) and the excitation and recombination process, $Cu^{2+} + h\nu \leftrightarrow (Cu^+, h^+_{VB})$, activates the SGE with high intensity. When the $Zn_i$ were introduced, due to hybridization between $Zn_i$ and Cu ions, $Cu^{2+}$ ions transformed from the paramagnetic state to the ferromagnetic state. As $Zn_i{:}Cu^{2+}{:}ZnO \leftrightarrow Zn_i^+{:}Cu^+{:}ZnO$ becomes the main CTT process, SGE is consequently diminished.

In conclusion, the concentration of shallow donors ($Zn_i$) is the trigger, which can be manipulated by sequential annealings in Zn vapor and oxygen ambience. Its variation

not only directly causes the transition between PM and FM accompanied by different CTTs but also, to our surprise, modified the well-known SGE indirectly. Nonetheless, in order to confirm our conclusion, further work still needs to be done, such as measuring the exact donor concentration in transport experiments and finding direct proof of the $Zn_i$–$Cu_{Zn}$ hybridization by studying MCD.

## 5. Conclusions

We have synthesized room temperature ferromagnetic Cu-doped ZnO NWs and ascribed the larger proportion of the magnetic moment in as-grown samples to the nanophase of CuO, which was readily ignored in many experiments. However, comparative annealing experiments in Zn vapor and oxygen ambience respectively constitute a simple and effective method for discerning such extrinsic sources. Furthermore, the weaker but intrinsic FM in such samples was found to be reversibly changed by the successive Zn–$O_2$ annealing, which was accompanied by adjustable photoluminescence. The study reveals that CTTs play an important role in tuning both the magnetic and optical properties of Cu-doped ZnO systems, for the first time. It also provides strong experimental evidence for the intrinsic shallow donors ($Zn_i$) mediating high $T_c$ ferromagnetism and suggests the possibility of using *ex situ* modifications to manipulate the magnetic and optical properties of DMSs, which may lay a foundation for their application in spintronics based devices. We believe that our work will contribute to significant judgments and understanding of the origin of RTFM in other DMSs systems, besides Cu-doped ZnO.

## Acknowledgments

This work was supported by the NSFC (90606023, 10574003, 20731160012, 10732040), the 973 program (2007CB936202/04, 2009CB623703) of China and NSFC/RGC (NHKUST615/06). We are also grateful to Mrs Chen who helped with the magnetic measurements.

## References

[1] Ohno H 1998 *Science* **281** 951
[2] Wolf S A, Awschalom D D, Buhrman R A, Daughton J M, von Molnar S, Roukes M L, Chtchelkanova A Y and Treger D M 2001 *Science* **294** 1488
[3] Dietl T, Ohno H, Matsukura F, Cibert J and Ferrand D 2000 *Science* **287** 1019
[4] Sato K and Katayama-Yoshida H 2002 *Semicond. Sci. Technol.* **17** 367
[5] Matsumoto Y, Murakami M, Shono T, Hasegawa T, Fukumura T, Kawasaki M, Ahmet P, Chikyow T, Koshihara S and Koinuma H 2001 *Science* **291** 854
[6] Pearton S J, Norton D P, Ip K, Heo Y W and Steiner T 2004 *J. Vac. Sci. Technol.* B **22** 932
[7] Kittilstved K R, Norberg N S and Gamelin D R 2005 *Phys. Rev. Lett.* **94** 147209
[8] Clavel G, Willinger M G, Zitoun D and Pinna N 2007 *Adv. Funct. Mater.* **17** 3159
[9] Dietl T, Ohno H and Matsukura F 2001 *Phys. Rev.* B **63** 195205
[10] Kaminski A and Das Sarma S 2002 *Phys. Rev. Lett.* **88** 247202
[11] Coey J M D, Venkatesan M and Fitzgerald C B 2005 *Nat. Mater.* **4** 173
[12] Ueda K, Tabata H and Kawai T 2001 *Appl. Phys. Lett.* **79** 988
[13] Lim S W, Jeong M C, Ham M H and Myoung J M 2004 *Japan J. Appl. Phys.* **43** L280
[14] Saeki H, Tabata H and Kawai T 2001 *Solid State Commun.* **120** 439
[15] Venkatesan M, Fitzgerald C B, Lunney J G and Coey J M D 2004 *Phys. Rev. Lett.* **93** 177206
[16] Schwartz D A and Gamelin D R 2004 *Adv. Mater.* **16** 2115
[17] Khare N, Kappers M J, Wei M, Blamire M G and MacManus-Driscoll J L 2006 *Adv. Mater.* **18** 1449
[18] Yan Z, Ma Y, Wang D, Wang J, Gao Z, Wang L, Yu P and Song T 2008 *Appl. Phys. Lett.* **92** 081911
[19] Herng T S, Lau S P, Yu S F, Chen J S and Teng K S 2007 *J. Magn. Magn. Mater.* **315** 107
[20] Chakraborti D, Trichy G R, Prater J T and Narayan J 2007 *J. Phys. D: Appl. Phys.* **40** 7606
[21] Herng T S, Lau S P, Yu S F, Yang H Y, Teng K S and Chen J S 2007 *J. Phys.: Condens. Matter* **19** 356214
[22] Kundaliya D C *et al* 2004 *Nat. Mater.* **3** 709
[23] Ando K, Saito H, Zayets V and Debnath M C 2004 *J. Phys.: Condens. Matter* **16** S5541
[24] Goennenwein S T B, Wassner T A, Huebl H, Brandt M S, Philipp J B, Opel M, Gross R, Koeder A, Schoch W and Waag A 2004 *Phys. Rev. Lett.* **92** 227202
[25] Wei M, Braddon N, Zhi D, Midgley P A, Chen S K, Blamire M G and MacManus-Driscoll J L 2005 *Appl. Phys. Lett.* **86** 072514
[26] Buchholz D B, Chang R P H, Song J H and Ketterson J B 2005 *Appl. Phys. Lett.* **87** 082504
[27] Ye L H, Freeman A J and Delley B 2006 *Phys. Rev.* B **73** 33203
[28] Huang L M, Rosa A L and Ahuja R 2006 *Phys. Rev.* B **74** 75206
[29] Chakraborti D, Trichy G, Narayan J, Prater J T and Kumar D 2007 *J. Appl. Phys.* **102** 113908
[30] Hou D L, Ye X J, Meng H J, Zhou H J, Li X L, Zhen C M and Tang G D 2007 *Appl. Phys. Lett.* **90** 142502
[31] Punnoose A, Magnone H, Seehra M S and Bonevich J 2001 *Phys. Rev.* B **64** 174420
[32] Sudakar C, Thakur J S, Lawes G, Naik R and Naik V M 2007 *Phys. Rev.* B **75** 054423
[33] Xing G Z *et al* 2008 *Adv. Mater.* **20** 3521
[34] Garcia M A *et al* 2007 *Nano Lett.* **7** 1489
[35] Yuhas B D, Fakra S, Marcus M A and Yang P D 2007 *Nano Lett.* **7** 905
[36] Buffat P and Borel J P 1976 *Phys. Rev.* A **13** 2287
[37] Liu L Q, Xiang B, Zhang X Z, Zhang Y and Yu D P 2006 *Appl. Phys. Lett.* **88** 063104
[38] Wang X F, Xu J B, Cheung W Y, An J and Ke N 2007 *Appl. Phys. Lett.* **90** 212502
[39] Moulder J F, Stickle W F, Sobol P E and Bomben K D 1992 *Handbook of X-Ray Photoelectron Spectroscopy* (Eden Prairie, MN: Perkin Elmer)
[40] Scrocco M 1979 *Chem. Phys. Lett.* **63** 52
[41] Vanheusden K, Seager C H, Warren W L, Tallant D R and Voigt J A 1996 *Appl. Phys. Lett.* **68** 403
[42] Kouklin N 2008 *Adv. Mater.* **20** 2190
[43] Meyer B K *et al* 2004 *Phys. Status Solidi* b **241** 231
[44] Dingle R 1969 *Phys. Rev. Lett.* **23** 579
[45] Vanheusden K, Warren W L, Seager C H, Tallant D R, Voigt J A and Gnade B E 1996 *J. Appl. Phys.* **79** 7983
[46] Djurisic A B, Choy W C H, Roy V A L, Leung Y H, Kwong C Y, Cheah K W, Rao T K G, Chan W K, Lui H T and Surya C 2004 *Adv. Funct. Mater.* **14** 856
[47] Broser I J, Germer R K F, Schulz H J E and Wisznewski K P 1978 *Solid-State Electron.* **21** 1597
[48] Dean P J, Robbins D J, Bishop S G, Savage J A and Porteous P 1981 *J. Phys. C: Solid State Phys.* **14** 2847
[49] Herng T S, Lau S P, Yu S F, Yang H Y, Ji X H, Chen J S, Yasui N and Inaba H 2006 *J. Appl. Phys.* **99** 086101

[50] Tiwari A, Snure M, Kumar D and Abiade J T 2008 *Appl. Phys. Lett.* **92** 062509
[51] Sundaresan A, Bhargavi R, Rangarajan N, Siddesh U and Rao C N R 2006 *Phys. Rev.* B **74** 161306
[52] Wahl U, Rita E, Correia J G, Alves E and Soares J G 2004 *Phys. Rev.* B **69** 012102
[53] Rubi D, Fontcuberta J, Calleja A, Aragones L, Capdevila X G and Segarra M 2007 *Phys. Rev.* B **75** 155322
[54] Meyer B K, Sann J, Hofmann D M, Neumann C and Zenner A 2005 *Semicond. Sci. Technol.* **20** S62
[55] Sann J, Stehr J, Hofstaetter A, Hofmann D M, Neumann A, Lerch M, Haboeck U, Hoffmann A and Thomsen C 2007 *Phys. Rev.* B **76** 195203
[56] Fujiwara H and Kondo M 2005 *Phys. Rev.* B **71** 075109
[57] Ogata K, Sakurai K, Fujita S, Fujita S and Matsushige K 2000 *J. Cryst. Growth* **214** 312
[58] Look D C, Hemsky J W and Sizelove J R 1999 *Phys. Rev. Lett.* **82** 2552
[59] Markevich I V, Kushnirenko V I, Borkovska L V and Bulakh B M 2006 *Phys. Status Solidi* c **3** 942
[60] Kittilstved K R, Schwartz D A, Tuan A C, Heald S M, Chambers S A and Gamelin D R 2006 *Phys. Rev. Lett.* **97** 037203
[61] Kittilstved K R, Liu W K and Gamelin D R 2006 *Nat. Mater.* **5** 291
[62] Schulz H J and Thiede M 1987 *Phys. Rev.* B **35** 18
[63] Garces N Y, Wang L, Bai L, Giles N C, Halliburton L E and Cantwell G 2002 *Appl. Phys. Lett.* **81** 622